

# Experimental and Theoretical Analysis on Mild Steel Corrosion Inhibition by Two Novel Compounds (FD and ACP) in Acidic Media

Vidyadharani Gopalakrishnan,<sup>1</sup> Anand Balasubramanian,<sup>2</sup>  
Loganathan Subramanian,<sup>2</sup> Rabiul Ibraheem Muhammed,<sup>3</sup>  
Rajni Garg<sup>4</sup> and Nnabuk Okon Eddy<sup>3\*</sup>

<sup>1</sup>Department of Microbiology, Valiammal College for Women,  
Chennai, Tamilnadu, India

<sup>2</sup>Department of Chemistry, Sir Theagaraya College, Chennai, Tamilnadu, India

<sup>3</sup>Department of Pure and Industrial Chemistry, University of Nigeria,  
Nsukka, Enugu State Nigeria

<sup>4</sup>R&D Department, Institute of Sci-Tech Affairs, Mohali, Punjab, India

\*Corresponding author: okon.nnabuk@unn.edu.ng

Received 26/11/2021; accepted 10/03/2022

<https://doi.org/10.4152/pea.2023410304>

---

## Abstract

Two novel synthesized compounds (FD and ACP) have been applied as inhibitors for MS corrosion in HCl and H<sub>2</sub>SO<sub>4</sub> solutions. Gravimetric, PDP, EIS, SEM and theoretical approaches were employed for the investigation of FD and ACP synthesized compounds IE%. Their corrosion IE% and calculated quantum chemical properties were comparable to each other, and indicated that ACP is a slightly less effective inhibitor than FD in HCl and H<sub>2</sub>SO<sub>4</sub> solutions. Langmuir's, Temkin's, Frumkin's and Freundlich's adsorption isotherms were used for describing the inhibitors adsorption behavior. The adsorption was spontaneous and followed a mixed mechanism, but with initial physisorption. Polarization data revealed that the inhibitors were more cathodic, because they tended to enforce MS HER retardation. The inhibitors decreased the electrolyte impedance, while R<sub>ct</sub> increased. The adsorption mechanism was influenced by the protonation and solvation environment, and it was concentrated within the heteroatoms and the aromatic systems. Calculated quantum parameters agreed effectively with the obtained experimental results, while FF indices were useful for predicting the nucleophilic and electrophilic attacks positions.

**Keywords:** ACP, adsorption isotherm, corrosion, EIS, FD, IE (%), MS and PDP.

---

## Introduction\*

In many industries, corrosion is a major threat to the infrastructures, and also tends to affect the GDP of a nation, due to the economic costs associated with it. Based on the recent GDP growth rate, the Indian government is losing about 2.4% of its economy, due to metals and alloys corrosion [1]. In Nigeria, corrosion economic

---

\* The abbreviations and symbols definition lists are in pages 243-244.

costs in the oil industry were estimated to be from 3 to 4% of the country's GDP [2], while, in South Africa, they were calculated in the range from 3 to 5%, and closely related to the global losses of \$255 billion [3]. MS is an iron and carbon alloy, being the major metal in several industrial installations [4]. However, within most of these industries, activities such as acid cleaning, etching, engraving and others, can accelerate MS CR, especially in acidic or basic environments [5-10]. Approaches to protecting metals against corrosion damages are varied, but include methods such as coating, electroplating, painting/greasing, cathodic/anodic protection and the use of corrosion inhibitors [11-14]. Inhibitors can be added to the corrosive substance in minute C, to protect metals against corrosion, through the initial adsorption mechanism [15, 16]. Most compounds employed as corrosion inhibitors are required to be biodegradable, less expensive, non-toxic and simple to handle [17]. The above-listed properties are valuable, and have positioned the use of corrosion inhibitors as one of the greatest alternatives for metal corrosion prevention [18].

The choice or design of a corrosion inhibitor is based on several chemical considerations, but the basic ones are the possession of heteroatoms, pi-electron or conjugated systems, high molecular weight, aromatic systems, multiple bonds, etc. [19]. Given the depth of knowledge that is available for guiding the choice of new ecofriendly inhibitors synthesis, several compounds have been explored for their corrosion IE (%) [18]. Some literature on the usage of carboxamide derivatives as corrosion inhibitors is available. For example, Dadgarinezhad and Daghael [20] explored the corrosion inhibition potential of 2-phenyl-1-hydrazine carboxamide in  $H_3PO_4$ , and observed that the adsorption mechanism obeyed the Langmuir's isotherm. Chafiq *et al.* [21] reported (E)-2-(4-(2-(methyl(pyridine-2-yl)amino)ethoxy) benzylidene)hydrazine-1-carboxamide as a cost-effective and efficient corrosion inhibitor, with maximum IE (%) of 97%, at a C of 0.005 M. Their experimental findings were in good agreement with data generated from theoretical calculations. Other related works about corrosion inhibitors have also been documented on 2-(1-(2-oxo-2H-chromen-3-yl) rthylidene) hydrazine carboxamide, for Zn-Al alloy in HCl solutions [22], and salicylaldehyde-based Schiff bases of semicarbazide and p-toluidine, for MS in an acidic medium [7]. On the other hand, studies on the inhibitive properties of pyridine substituted amines are much scanty, except some reports that include the study conducted by Farahati *et al.* [23], who found that 4-(pyridic-3-yl) thiazol-2-amine was an effective and eco-friendly inhibitor for Cu corrosion in HCl.

In continuation of this novel exercise, we have successfully synthesized and applied two aromatic compounds (FD and ACP), as inhibitors for MS corrosion in acidic media. Despite the other relevant works, the use of these compounds as inhibitors for MS corrosion in HCl and  $H_2SO_4$  has not been previously reported. The current study researched the synthesis and corrosion inhibitive properties of these compounds, at 303 K, which is the approximate temperature in which most fluids are handled in industries. Although most industrial fluids pH values are relatively acidic, the study was conducted under simulated acidic conditions, at 1 M. The compounds chosen for the present study have hetero atoms, pi-electrons and aromatic rings, and were expected to exhibit corrosion IE (%).

## Experimental

### Material preparation

A commercially available MS sheet was procured and cut into coupons of the required dimensions  $5 \times 1$  and  $1 \times 1 \times 1$  cm, for gravimetric and electrochemical experiments, respectively. MS composition was (%): C = 0.014; Si = 0.007; Mn = 0.195; S = 0.014; P = 0.010; Ni = 0.014; Mo = 0.014; Cr = 0.041 and Fe = 99.691. Each coupon was polished using varying grades (120-1200 grits) of emery sheets. They were further cleaned with ethanol, for degreasing, and rinsed with acetone, before being stored in a desiccator.

### FD preparation

At a temperature from 0 to 5 °C, 0.02 M aniline were dissolved in glacial acetic acid and 0.5 mL HCl. The mixture was diazotized with 0.2 g sodium nitrite, under constant stirring, while 0.01 M semi-carbazone was slowly added, and allowed to cool overnight. The resulting solution was decanted into cold water, and the precipitated crystals were separated and recrystallized with ethanol. The recrystallized crystals were used to prepare formazan of p-dimethyl amino benzaldehyde, by dissolving 10 mg of this compound. FD C needed for the corrosion study were prepared through serial dilution.

### ACP preparation

ACP was synthesized using the method described by Zhang *et al.* [24]. A stock solution of ACP was made by dissolving 10 mg of it in 100 mL of the test solution, and carrying out serial dilution to obtain the desired C.

### WL method

WL experiments were conducted by completely immersing the weighed MS specimens into various beakers containing different FD and ACP C. Each MS coupon was taken out from the solution, following 24 h of immersion, washed, and returned to the solution after weighing. The experiments used a thermostated water bath (303 K), and they were repeated and concluded in seven days. MS CR, FD and ACP IE (%) and  $\theta$  were computed by the measured values substitution into Equations 1, 2 and 3, respectively [25]:

$$\text{Corrosion rate (mm/y)} = \frac{87.6\Delta w}{A\rho t} \quad (1)$$

$$\%IE = \frac{CR_b - CR_{inh}}{CR_b} \times \frac{100}{1} \quad (2)$$

$$\theta = \% \frac{IE}{100} = \frac{CR_b - CR_{inh}}{CR_b} \quad (3)$$

where  $\Delta w$ , A and  $\rho$  are the MS coupons WL, cross-sectional area and density, and t is the contact period, respectively.

### PDP study

The MS sample, SC and Pt were used as WE, RE and AE, respectively, in the PDP cell. The electrolyte was the respective corrosive acid (HCl or H<sub>2</sub>SO<sub>4</sub>). PDP

measurements were accomplished in the potential ranges from -1000 to 250 mV and from 1000 to 2000 mV, at a SR of 0.5 mV/s<sup>-1</sup>. Data obtained from the PDP cell were E<sub>corr</sub>, I<sub>corr</sub>, β<sub>c</sub> and β<sub>a</sub>. From PDP measurements, FD and ACP IE% were computed by the following equation [25]:

$$IE\% = \frac{i_{\text{corr}}^0 - i_{\text{corr}}}{i_{\text{corr}}^0} \times \frac{100}{1} \quad (4)$$

where I<sub>corr</sub><sup>0</sup> and I<sub>corr</sub> are the corrosion current without and with inhibitor. LPR experiment was also carried out in the same electrochemical cell. From R<sub>p</sub> calculated values, IE% was evaluated by using the following equation [26]:

$$IE\% = \frac{R_{p(i)} - R_p}{R_{p(i)}} \times \frac{100}{1} \quad (5)$$

where R<sub>p(i)</sub> and R<sub>p</sub> are polarization resistance without and with inhibitor, respectively.

### **EIS**

EIS study was performed using an electrochemical analyzer, and the conventional three electrodes that were similar to those used in the PDP experiment. A steady-state potential wave was first obtained, and sine wave AC signal of 10 mV amplitude was overlaid, in order to obtain OCP. This was conducted using the frequency range from 100 kHz to 10 MHz, in order to obtain values for the real (Z') and imaginary (Z'') parts. C<sub>dl</sub> was calculated by the following equation [27]:

$$C_{dl} = \frac{1}{2\pi f_{\text{max}} R_{ct}} \quad (6)$$

where f<sub>max</sub> is the frequency at Z'' value. IE% was calculated by using the following equation 7 [28]:

$$IE\% = \frac{R_{ct(i)} - R_{ct}}{R_{ct(i)}} \times \frac{100}{1} \quad (7)$$

where R<sub>ct</sub> and R<sub>ct(i)</sub> are the charge transfer resistance without and with inhibitor respectively.

### **SEM**

Morphological analysis of the corroded MS surface (without and with inhibitor) was carried out at Metallurgical and Material Department, NIT Tiruchi, India, using SEM (Model- HITACHI S3000H, Japan). The MS coupons were immersed in the test solutions (without and with 35% inhibitors C), and allowed to stand for seven days, before they were withdrawn for SEM analysis.

### **Computational calculations**

Chemical structures were drawn with the aid of ChemBio 12.0 software, and the structured produced were saved as a SDF input file, for structural optimization. DFT calculations were performed with a /631G\*\* basis set and B3LYP hybrid functional. FMO graphs plotting was also performed at this level of theory. Calculations were performed for both aqueous and gaseous phases. FF calculations

were carried out using electrostatic E, MC and NBOC. In order to determine the interaction between the inhibitor and the MS surface, Monte Carlo simulation was performed using HyperChem software.

## Results and discussion

### WL method

The MS coupons CR was observed to decline with increasing ACP and FD C, as shown in Table 1.

**Table 1.** MS CR, ACP and FD  $\theta$  and IE (%) with various C.

System	CR (mm/y)	$\theta$	IE(%)	CR mm/y	$\theta$	IE %
	<b>1.0 M HCl</b>			<b>1.0 M H<sub>2</sub>SO<sub>4</sub></b>		
Blank	29.5715	-	-	30.9832	-	-
7% FD	13.9385	0.5287	52.87	18.5786	0.4004	40.04
14% FD	11.023	0.6272	62.72	14.0184	0.5475	54.75
21% FD	8.3217	0.7186	71.86	10.2385	0.6695	66.95
28% FD	6.231	0.7893	78.93	7.7921	0.7485	74.85
35% FD	4.8987	0.8343	83.43	5.6743	0.8169	81.69
Blank	29.5715	-	-	30.9832	-	-
7 % ACP	24.2961	0.1784	17.84	21.0269	0.3213	32.13
14% ACP	19.4666	0.3417	34.17	17.6091	0.4317	43.17
21% ACP	14.6371	0.5050	50.50	12.631	0.5923	59.23
28% ACP	9.9562	0.6633	66.33	10.2534	0.6691	66.91
35% ACP	6.9099	0.7663	76.63	5.8697	0.8106	81.06

MS coupons CR were 29.5715 and 30.9832 mmpy, in 1 M HCl and H<sub>2</sub>SO<sub>4</sub>, respectively. As ACP C was increased from 7 to 35%, CR decreased from 13.9385 to 4.8982 mmpy, in HCl, which corresponded to an IE (%) increase from 52.87 to 83.43%. In H<sub>2</sub>SO<sub>4</sub>, CR decreased from 18.5786 to 5.6743 mmpy, while the corresponding IE (%) rose from 40.04 to 81.69%. This reveals that MS coupons CR in 1.0 M H<sub>2</sub>SO<sub>4</sub> was higher than that in 1.0 M HCl, because the former is a stronger dibasic acid than the latter. Similarly, FD IE (%) for MS coupons CR in HCl was found to be slightly better than that in H<sub>2</sub>SO<sub>4</sub>. ACP exhibited relatively lower corrosion IE (%) than that of FD, within the studied C range (from 7 to 35%). ACP demonstrated the capacity to reduce MS coupons CR from 24.2961 to 6.9099 mmpy in 1 M HCl, and from 21.0269 to 5.8697 mmpy in H<sub>2</sub>SO<sub>4</sub>. ACP seems to be a better inhibitor for MS coupons corrosion in H<sub>2</sub>SO<sub>4</sub> than in HCl. This may be because H<sub>2</sub>SO<sub>4</sub> tends to form a passivating layer on the metal surface, through tetraoxosulphate (VI) ions adsorption.

Further, the observed trend for the changes in corrosion IE (%) concerning the inhibitors and the acidic media was: FD in HCl > FD in H<sub>2</sub>SO<sub>4</sub> > ACP in H<sub>2</sub>SO<sub>4</sub> > ACP in HCl (Fig. 1). Considering the two inhibitors chemical structures, it is obvious that FD has more functional corrosion inhibition enhancing properties than those of ACP, including two aromatic rings and several heteroatoms, with multiple bonds and higher molecular mass. Therefore, the observed results are consistent with the compounds chemical structures.

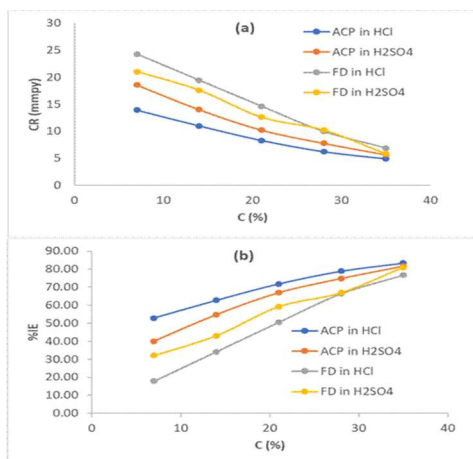


Figure 1. Variation of (a) MS CR and (b) ACP and FD IE (%) with various C.

MS CR, and instantaneous ACP and FD IE (%), with eight 4 h intervals (from 4 to 24 h), were also calculated, and the obtained results are presented in Table 2.

Table 2. Instantaneous ACP and FD CR and IE(%).

Time (h)	ACP				FD			
	CR mmpy		IE (%)		CR mmpy		IE (%)	
	1 M HCl	1 M H <sub>2</sub> SO <sub>4</sub>	1 M HCl	1 M H <sub>2</sub> SO <sub>4</sub>	1 M HCl	1 M H <sub>2</sub> SO <sub>4</sub>	1 M HCl	1 M H <sub>2</sub> SO <sub>4</sub>
4	4.5210	5.5241	75.64	79.71	6.8987	5.5432	77.21	81.98
8	4.2891	5.4001	76.78	81.75	6.7654	5.5098	78.37	83.84
12	4.0051	5.3198	77.92	83.79	6.4589	5.4678	79.53	85.70
16	3.7895	5.2779	79.06	85.83	6.2897	5.4318	80.69	87.56
20	3.4879	5.0988	80.20	87.87	6.1544	5.4218	81.85	89.42
24	3.4870	5.0897	80.77	88.89	6.1320	5.4119	82.43	90.35

The recorded results clearly show that the instantaneous ACP and FD IE (%) were much better than those of other inhibitors. Similar results have been reported for some effective corrosion inhibitors [29].

The instantaneous MS coupons CR, and ACP and FD IE (%) in the acidic media linearly decreased with time (Fig. 2), which implies that MS corrosion in both media was uniform.

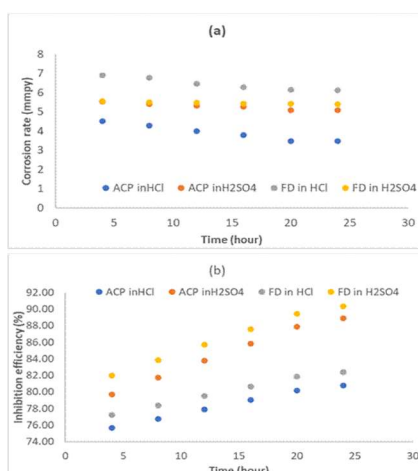


Figure 2. Time variation with instantaneous: (a) MS CR in 1 M HCl and 1 M H<sub>2</sub>SO<sub>4</sub>; and (b) ACP and FD IE (%).

Time changes with MS C in the corrosive media were also monitored through WL measurement, and the obtained data were used to test for the best suited kinetic plots. The requirements for a first-order kinetic were satisfied:

$$\log\left(\frac{[MS]_t}{[MS]_0}\right) = -k_1 t \tag{8}$$

where  $[MS]_0$  and  $[MS]_t$  are the alloy initial and final C in the corrosive media, t is time and  $k_1$  is the first-order rate constant.

From the plots of  $\log\left(\frac{[Fe]_t}{[Fe]_0}\right)$  against t (figure not shown), half-life ( $t_{1/2} = \frac{0.693}{k_1}$ ) was estimated (Table 3).

**Table 3.** Kinetic parameters for MS CR in 1 M HCl and 1 M H<sub>2</sub>SO<sub>4</sub> without and with ACP and FD.

Time (h)	ACP				FD			
	Rate constant K*10 <sup>-1</sup>		t <sub>1/2</sub>		Rate constant K*10 <sup>-1</sup>		t <sub>1/2</sub>	
	1 M HCl	1 M H <sub>2</sub> SO <sub>4</sub>	1 M HCl	1 M H <sub>2</sub> SO <sub>4</sub>	1 M HCl	1 M H <sub>2</sub> SO <sub>4</sub>	1 M HCl	1 M H <sub>2</sub> SO <sub>4</sub>
4	0.3674	0.4194	188.6	165.2	0.3377	0.4302	205.2	161.0
8	0.1902	0.2125	364.3	326.1	0.1712	0.2158	404.7	321.1
12	0.1325	0.1429	523.0	484.9	0.1180	0.1445	587.2	479.5
16	0.1028	0.1076	674.1	644.0	0.0902	0.1088	768.2	636.9
20	0.0864	0.0878	802.0	789.2	0.0732	0.0871	946.7	795.6
24	0.0720	0.0732	962.5	946.7	0.0611	0.0726	1134.2	954.5

The presented results reveal that the inhibitors effectively extended MS half-life up to 963, 947, 1134 and 955 h, with ACP and FD in HCl and H<sub>2</sub>SO<sub>4</sub>, respectively.

**Adsorption/thermodynamic study**

ACP and FD characteristics against MS corrosion in HCl and H<sub>2</sub>SO<sub>4</sub> solutions are essential parameters in their interaction level, inhibition mechanisms and other inhibitory roles features. The adsorption linear fitness results indicated that the mechanism best fitted Langmuir’s, Temkin’s, Frumkin’s, and Freundlich’s isotherms, which are expressed in Equations 9 to 12, respectively [30, 31].

$$\ln\left(\frac{C}{\theta}\right) = \ln\left(\frac{1}{k_{ad(LM)}}\right) + \ln C \tag{9}$$

$$\theta = \frac{1}{2\alpha} \ln k_{ad(TK)} - \frac{1}{2\alpha} \ln C \tag{10}$$

$$n\left\{[C] \times \left(\frac{\theta}{1-\theta}\right)\right\} = \ln k_{ad(FK)} + 2\alpha \tag{11}$$

$$\ln(\theta) = \ln k_{ad(FR)} + \frac{1}{n} \ln C \tag{12}$$

where a is Temkin’s interaction parameter, α is the lateral interaction factor describing the adsorption layer and 1/n is the Freundlich’s constant for the adsorption intensity or surface heterogeneity. Langmuir’s, Temkin’s, Frumkin’s and Freundlich’s isotherms are presented in Table 4.

The plots fitness was excellently supported by R<sup>2</sup> high values. The various adsorption constants for the isotherms are illustrated in Fig. 3.

ΔG<sup>o</sup><sub>ads</sub> for the inhibitors adsorption was calculated from the respective k<sub>ads</sub> values using equation 13 [32]:

$$\Delta G_{ads}^0 = -RT \ln(55.5 k_{ads}) \tag{13}$$

where R is the gas constant, T is temperature and 55.5 is the molar heat of water adsorption.

**Table 4.** Parameters for ACP and FD adsorption onto the MS surface in HCl and H<sub>2</sub>SO<sub>4</sub> solutions.

Isotherms and parameters	FD in 1 M HCl	FD in 1 M H <sub>2</sub> SO <sub>4</sub>	ACP in 1 M HCl	ACP in 1 M H <sub>2</sub> SO <sub>4</sub>
<b>Langmuir's</b>				
Slope	0.7107	0.5525	0.0787	0.4267
Intercept	1.2104	1.7815	3.5064	2.2866
$\Delta G^{\circ}_{ads}$ kJ/mol	-12.25	-18.02	-35.48	-23.14
R <sup>2</sup>	0.9993	-0.9990	0.8093	0.9732
<b>Temkin's</b>				
Slope	0.1930	0.2599	0.3678	0.2954
Intercept	0.1394	-0.1181	-0.5768	-0.2926
$\alpha$	2.5907	1.9238	1.3594	1.6926
$\Delta G^{\circ}_{ads}$ kJ/mol	-11.94	-8.97	-6.17	-7.62
R <sup>2</sup>	0.9861	0.9935	0.9682	0.9456
<b>Frumkin's</b>				
Slope	9.9730	8.3148	7.1492	7.6254
Intercept	-3.1720	-1.7737	-0.6659	-1.1103
$\alpha$	4.9865	4.1574	3.5746	3.8127
$\Delta G^{\circ}_{ads}$ kJ/mol	-21.27	-56.50	-84.40	-73.21
R <sup>2</sup>	0.9983	0.9992	0.9912	0.9932
<b>Freundlich's</b>				
Slope	0.2893	0.4475	0.9213	0.5733
Intercept	-1.2104	-1.7815	-3.5064	-2.2866
1/n	0.2893	0.4475	0.9213	0.5733
$\Delta G^{\circ}_{ads}$ kJ/mol	-70.69	-56.30	-12.85	-43.58
R <sup>2</sup>	0.9957	0.9985	0.9983	0.9850

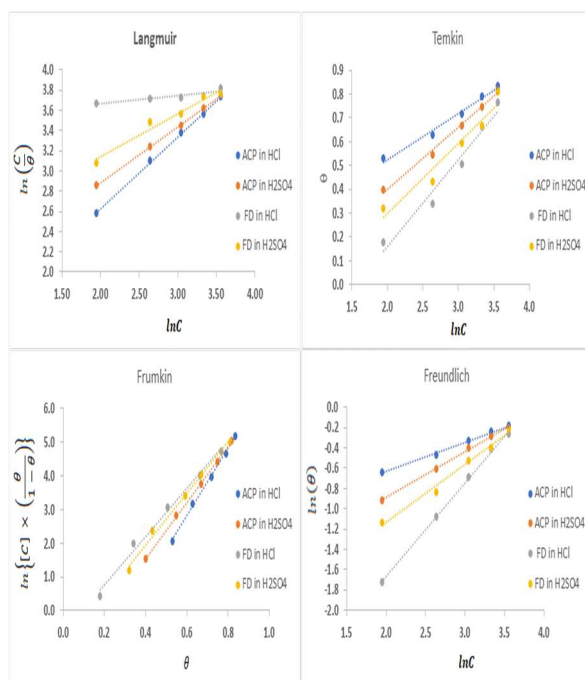


**Figure 3.** Isotherms for ACP and FD adsorption onto the MS surface.

The ideal Langmuir's isotherm describes a homogenous adsorption layer with no interaction between the adsorbed species. Since the expected slope value for the ideal

Langmuir’s isotherm is unity (Equation 9), there was an observable deviation concerning ACP and FD adsorption onto the MS surface (slope > 1 for ACP and FD). Hence, there was an interaction between the adsorbed species. The interaction parameters calculated through Temkin’s and Frumkin’s isotherms reflected the inhibitors adsorption behavior, since they were positive. In both cases, the interaction strength was most intense for FD in HCl.

The calculated  $\Delta G^{\circ}_{ads}$  (Table 4) values correspond to different adsorption mechanisms. For example, the Langmuir’s, Temkin’s, Frumkin’s and Freundlich’s models generated  $\Delta G^{\circ}_{ads}$  values of -12.25, -11.94, -21.27 and -70.29 kJ/mol, for FD in HCl, respectively.  $\Delta G^{\circ}_{ads}$  values lower than -20 kJ/mol and higher than -40 kJ/mol favor physical and chemical adsorption mechanisms, respectively. Free energy values from -20 to -40 kJ/mol often indicate a mixed adsorption mechanism. Therefore, the inhibitors adsorption onto the metal surface first underwent physisorption, and then chemisorption. Interestingly, Freundlich’s constant (1/n) was lower than unity, and supported chemisorption mechanism (unlike cooperative adsorption, which requires that 1/n should be greater than unity). Some levels of agreement between data obtained from the various isotherms were also observed, for example,  $\Delta G^{\circ}_{ads}$  values evaluated from Frumkin’s and Freundlich’s isotherms were -56.50 and -56.30 kJ/mol, respectively, for FD adsorption onto the MS surface (in H<sub>2</sub>SO<sub>4</sub>).

**Polarization studies**

PDP and LPR studies were also useful in ACP and FD IEs evaluation (Fig. 4).

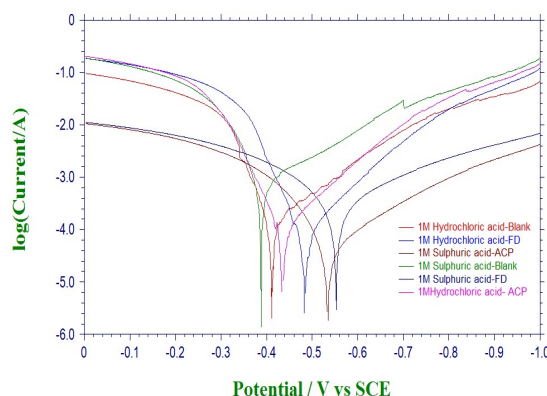


**Figure 4.** PDP plots for MS corrosion inhibition in HCl and H<sub>2</sub>SO<sub>4</sub> solutions, by ACP and FD.

Table 5 contains polarization data and calculated ACP and FD IE (%). The inhibitors addition to HCl and H<sub>2</sub>SO<sub>4</sub> led to an increase in E<sub>corr</sub> absolute value, while I<sub>corr</sub> decreased. This indicates that ACP and FD inhibited MS corrosion in the acidic media.

**Table 5.** PDP data for ACP and FD in 1 M HCl and H<sub>2</sub>SO<sub>4</sub>.

System	PDP						LPR	
	$\beta_c$ V/dec <sup>-1</sup>	$\beta_a$ V/dec <sup>-1</sup>	E <sub>Corr</sub> V	I <sub>Corr</sub> X 10 <sup>-4</sup> (A)	CR mmpy	IE(%)	R <sub>p</sub>	IE(%)
1 M HCl	5.593	18.793	-0.411	7.625	12.384	-	245.45	-
ACP in 1 M HCl	7.515	17.007	-0.436	2.315	5.679	69.63	977.58	74.89
FD in 1 M HCl	8.240	20.719	-0.483	1.910	7.015	74.95	1340.2	81.69
1 M H <sub>2</sub> SO <sub>4</sub>	4.015	15.354	-0.387	9.125	13.666	-	151.45	-
ACP in 1 M H <sub>2</sub> SO <sub>4</sub>	5.905	12.905	-0.532	2.493	7.241	72.67	705.62	78.54
FD in 1 M H <sub>2</sub> SO <sub>4</sub>	4.191	6.088	-0.554	1.870	6.985	79.50	576.37	73.72

The observed changes in  $\beta_c$  were more significant than those in  $\beta_a$ , which suggests that the inhibition process significantly retarded H reduction mechanism. It also implies that the anodic reaction was more favored than the cathodic one. Calculated differences in E were also greater than the threshold value (85 mV), confirming that the inhibitors are majorly anodic [33]. Further investigation of the inhibitors anodic character was made through the results obtained from the transfer coefficient calculations. The transfer coefficient can be calculated by the substitution of R values, temperature and Tafel slope, and by the number of electrons associated with the redox reaction, into equation 14:

$$\alpha = \frac{2.303RT}{anF} \tag{14}$$

where  $\alpha$  is the Tafel slope, n is the number of electrons in the redox reaction and F is Faraday’s constant. The Tafel slope was deduced from the following equation:

$$\beta = \frac{\beta_a\beta_c}{2.303(\beta_a + \beta_c)} \tag{15}$$

$\alpha$  calculated values are shown in Table 6. Generally, anodic reaction and cathodic polarization are favored when  $\alpha$  values are from 0.25 to less than 0.5, and close to 0.75, respectively. The presented results also confirmed that the inhibitors are majorly anodic, and suppress HER more than MS anodic dissolution.

**Table 6.** ACP and FD charge transfer coefficients and Tafel constant.

System	Charge transf. coef.	$\alpha$
1 M HCl	1.8716	0.0563
ACP in 1 M	2.2631	0.0681
FD in 1 M HCl	2.5599	0.0771
1 M H <sub>2</sub> SO <sub>4</sub>	1.3820	0.0416
ACP in 1 M	1.7591	0.0529
FD in 1 M	1.0778	0.0324

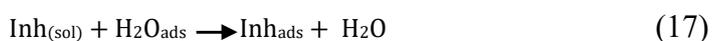
LPR study on the acidic solutions (Table 5) indicated that  $R_p$  was increased by ACP and FD, which imply that the inhibitors decreased CR in the acidic media. IE (%) calculated from PDP and LPR studies are consistent with each other, and with the instantaneous IE (%) presented in Table 2.

**EIS**

EIS measurements were also performed to study ACP and FD corrosion inhibition properties. The Nyquist plots generated from the EIS study are shown in Fig. 5, which reveals that the semicircle widened in FD presence, showing higher increment and better IE (%) than those from ACP. The phase angles approached 80°, implying that diffusion was not the rate control parameter.  $C_{dl}$  values can also be calculated through the following equation [34]:

$$C_{dl} = \gamma_0(\omega_{max})^{n-1} = \gamma_0(2\pi f_{max})^{n-1} \tag{16}$$

Corrosion inhibition may be thought of as the inhibitor displacing adsorbed water onto the metal surface (Equation 17):



In most cases, organic inhibitors have a lower dielectric constant and higher volume than water, and the relationship between  $C_{dl}$  and dielectric constant is given as follows:

$$C_{dl} = \frac{\epsilon \text{ and } \epsilon_0}{l} A \tag{17}$$

where  $\epsilon_0$  and  $\epsilon$  are the dielectric constant in vacuum and in the solution, respectively,  $l$  is  $C_{dl}$  thickness and  $A$  is the MS cross-sectional area.

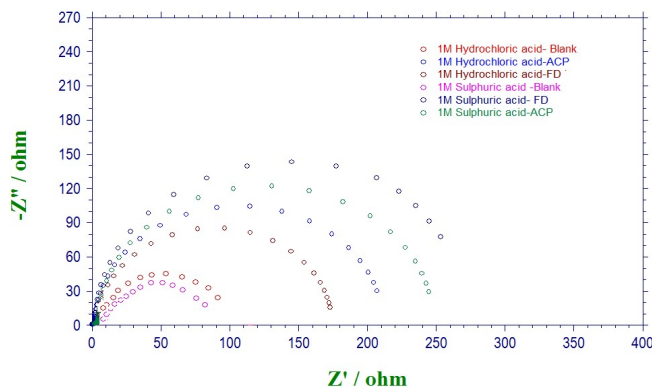


**Figure 5.** Nyquist plots for ACP and FD inhibition of MS corrosion in HCl and H<sub>2</sub>SO<sub>4</sub>.

From equation 18, it is evident that the higher the  $\epsilon$  value, the higher will be  $C_{dl}$ . Therefore, the replacement of the adsorbed water molecule (with a higher dielectric constant), on the metal surface, by an organic inhibitor (with a lower dielectric constant) will cause a reduction in  $C_{dl}$ , as shown in the results obtained for FD and ACP (Table 7). Thus, the observed decreasing trend in  $C_{dl}$  indicates that the inhibitors were adsorbed at the MS-solution interface. On the other hand, FD addition to the acidic solutions led to the highest increase in their  $R_{ct}$ . This can be ascribed to  $C_{dl}$  reduction and, hence, to MS corrosion inhibition by the formation of a protective film on its surface, through the inhibitors electrostatic attraction.

**Table 7.** AC impedance parameters of MS immersed in 1 M HCl and H<sub>2</sub>SO<sub>4</sub> without and with inhibitors.

System	$R_{ct}$ (ohm/cm <sup>2</sup> )	$C_{dl}$ ( $\mu F \times 10^{-5}$ )	IE (%)
1 M HCl	64.69	3.979	---
ACP in 1 M HCl	207.1	1.738	68.76
FD in HCl	269.4	1.280	75.98
1 M H <sub>2</sub> SO <sub>4</sub>	64.34	4.831	---
ACP in 1 M	242.7	1.447	73.48
FD in H <sub>2</sub> SO <sub>4</sub>	286.0	0.938	77.50

The radius of the semi-circle for the blank solutions is larger than those observed for ACP or FD in the corrosive media. This is due to the depressive capacitive loop (of which center is below the real axis) made by the impedance spectra, causing roughness and inhomogeneities at the MS surface.

**SEM**

Fig. 6 shows MS SEM in 1 M HCl and H<sub>2</sub>SO<sub>4</sub>, without and with ACP and FD. The micrographs reveal that the MS surface was intensely rough, but got smoother with ACP and FD, which have formed a protective coverage on it through adsorption.

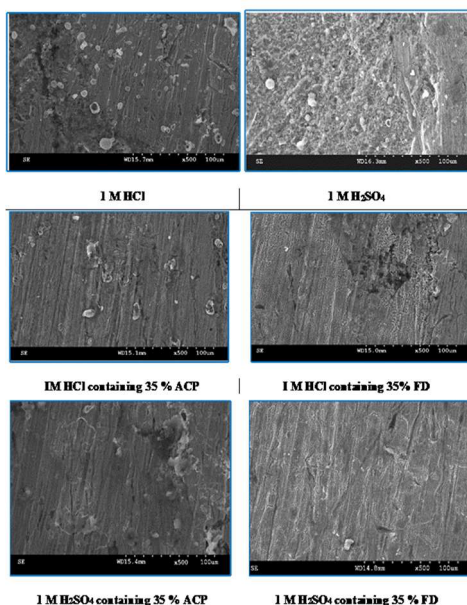


Figure 6. MS SEM in HCl and H<sub>2</sub>SO<sub>4</sub> solutions without and with ACP and FD.

### Quantum chemical study

#### Global reactivity

Semi-empirical parameters were calculated for ACP and FD in the gas phase. They included  $E_{HOMO}$ ,  $E_{LUMO}$ ,  $\Delta E$  and  $\mu$  (Table 8).

The reactivity of a corrosion inhibitor can be predicted from FMO theory, which states that LUMO is located in the electrophilic site. The theory requires the molecule reactivity to be a function of FMO energies. Consequently, reactivity (and, hence, adsorption) increases with higher  $E_{HOMO}$  value and with lower  $E_{LUMO}$  and  $\Delta E$  values.  $\Delta E$  is the measure of a compound  $\eta$  or  $\sigma$ , in terms of its tendency towards adsorption or reactivity [7]. Higher the  $\Delta E$ , higher the reactive molecules  $\sigma$  (hence, lower  $\eta$ ). Molecular  $\sigma$  and  $\eta$  are defined as follows [35]:

$$S = \frac{1}{E_{LUMO} - E_{HOMO}} \quad (18)$$

$$\eta = \frac{1}{2}(E_{LUMO} - E_{HOMO}) \quad (19)$$

IP and EA of an inhibitor are defined as  $E_{HOMO}$  and  $E_{LUMO}$  negative values, respectively, while  $\chi$  is defined as the inhibitor chemical E negative value, which can be calculated by IP and EA substitution into the following equation:

$$\chi = \frac{1}{2}(IP + EA) = \frac{1}{2}(-E_{HOMO} - E_{LUMO}) \quad (20)$$

$\Delta N$  from the inhibitor to the metal vacant d-orbital and the initial inhibitor-MS interaction were estimated using Equations 22 and 23, respectively:

$$\Delta N = \frac{(\chi_{Fe} - \chi_{inh})}{2(\eta_{Fe} + \eta_{inh})} \quad (21)$$

$$\Delta\phi = \frac{(\chi_{Fe} - \chi_{inh})^2}{4(\eta_{Fe} + \eta_{inh})} \quad (22)$$

Calculated values of all the variables obtained from Equations 17 to 21 are also presented in Table 8. The results favor FD as better corrosion inhibitor than ACP, because it has  $E_{HOMO}$ ,  $\Delta N$ ,

$\Delta\phi$ ,  $\sigma$ ,  $\chi$  and  $\mu$  higher values. Also, FD better IE (%) than that of ACP was supported by its observed  $\Delta E$  lower values. This theoretical proposal is in agreement with the results obtained for the average IE (%) of ACP and FD. Also, the relative closeness of the calculated global parameters between the two inhibitors explains why their IE (%) are also close to each other.

**Table 8.** Gas phase semi-empirical and associated parameters for ACP and FD.

Semi-empirical parameters	FD	ACP
$E_{\text{HOMO}}$ (eV)	-5.76	-5.86
$E_{\text{LUMO}}$ (eV)	-3.17	-2.18
$\Delta E$ (eV)	2.59	3.68
$\mu$ (debye)	6.02	5.86
$\sigma$	0.39	0.17
$\eta$	2.56	5.88
$\chi$	4.07	4.02
$\mu$	1.30	1.84
$\Delta N$	1.12695	0.8098
$\Delta\phi$	1.6509	1.2066

The corrosion inhibitor protonation is an essential step towards its adsorption, because higher fractions of inhibitor molecules are adsorbed in the protonated state. Energy minimization was first carried out on the inhibitors molecules, to identify the protonation sites, which were carboxyl oxygen and aromatic nitrogen in FD and ACP, respectively. Consequently, we calculated the two inhibitors protonation affinity, using the following Equation 24 [36]:

$$E_{\text{prot(aq)}} = E_{\text{prot-mol(aq)}} - E_{\text{neut-mol(aq)}} - E_{\text{prot-H}^+} \quad (23)$$

$$E_{\text{prot-mol(aq)}}, E_{\text{neut-mol(aq)}} \text{ and } E_{\text{prot-H}^+}$$

where  $E_{\text{prot(aq)}}$ ,  $E_{\text{neut}}$  and  $E_{\text{prot}}$  are the protonated inhibitor, neutral inhibitor and proton total energy, respectively. FD and ACP calculated PA values were 277.98 and 703.01 kJ/mol, respectively, which implies that the former can be easily protonated, because it requires lower energy than that of the latter. Therefore, FD IE (%) is expected to be better than that of ACP, as observed in the experimental results. Fig. 7 shows HOMO and LUMO optimized structures and gas-phase diagrams for ACP and FD.

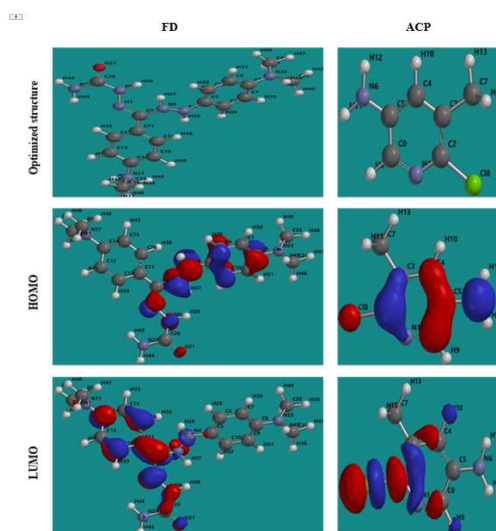


**Figure 7.** Inhibitors HOMO and LUMO optimized structures and gas-phase diagrams.

Fig. 8 shows similar diagrams for the inhibitors aqueous phase neutral and protonated forms. The diagrams reveal that the lobes are mostly concentrated in the benzene ring and on the heteroatoms, and that protonation seemed to enhance the inhibitors adsorption (especially FD), by increasing available active sites.

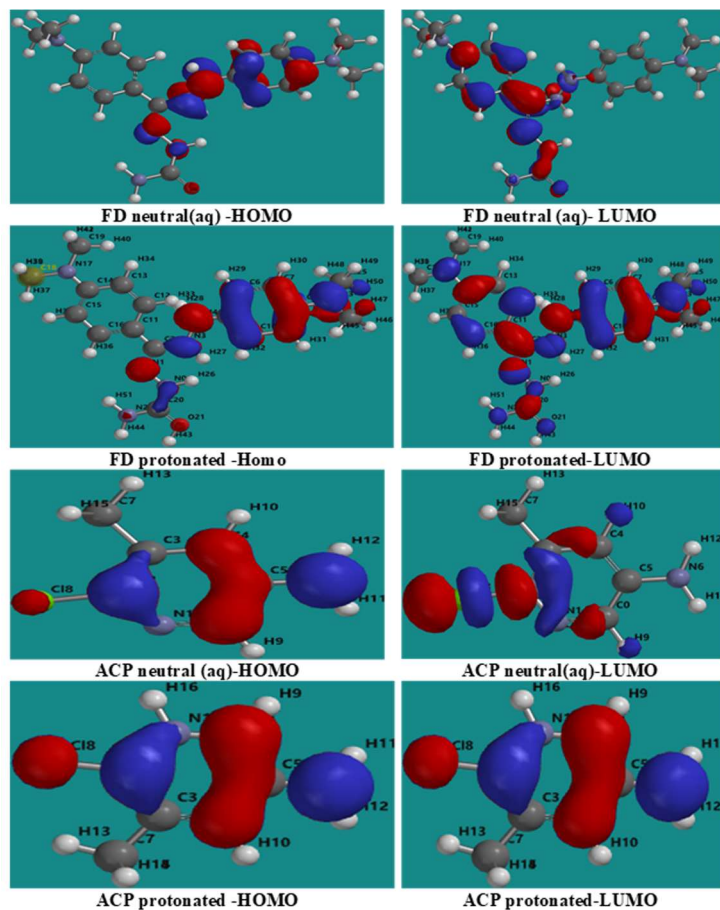


**Figure 8.** HOMO and LUMO aqueous phase neutral and protonated ACP and FD diagrams.

Recorded in Table 9 are FMO energies of neutral and protonated ACP and FD, in an aqueous solution.

**Table 9.** Aqueous phase FMO of neutral and protonated ACP and FD.

FMOs	FD (aqueous)		ACP (aqueous)	
	Neutral	Protonated	Neutral	Protonated
$E_{HOMO}$ (eV)	-5.03	-3.91	-5.66	-5.98
$E_{LUMO}$ (eV)	-2.38	-0.57	-2.38	-1.95
$\Delta E$ (eV)	2.65	3.34	3.28	4.03
$\mu$ (debye)	7.97	16.51	8.75	7.04

The results show more significant and favorable changes in the FMO of the FD protonated species than of that in the neutral species (in an aqueous medium). For example,  $E_{HOMO}$

increased, while ELUMO decreased, due to protonation. The contrary was observed for ACP inhibitors, which also explains why ACP IE (%) is lower than that of FD.

### LRD

Approaches to LRD analysis involve exploring the functions that can predict the molecules reactivity through their atoms. Some of the indices include charges on the molecules, FF, local  $\sigma$  and other parameters. FMO theory proposed that an electrophilic attack favors LUMO, while a nucleophilic attack favors HOMO. The electrons and charges involvement in the adsorption process can be simplified by  $\Delta N$  from HOMO to LUMO, which corresponds to nucleophilic and electrophilic attacks, respectively. The transfer process depends on  $\Delta E$  and other factors, such as electrons density in the respective sites, metal charge, etc. DFT was used to evaluate the condensed FF for the electrophilic and nucleophilic attacks, which can formally be defined according to the following equations [37]:

$$f_x^- = q_N - q_{N-1} \quad (24)$$

$$f_x^+ = q_{N+1} - q_N \quad (25)$$

where  $q_N$ ,  $q_{N-1}$  and  $q_{N+1}$  are the ground state charges of the neutral, positive and negative species, respectively. In this study, different FD and ACP charges were used for evaluating FF indices, including EPC, MAC and NOBC. The results are shown in Tables 10-15.

**Table 10.** ACP and FD EPC calculated FF parameters for the gas-phase.

FD				ACP			
Atom	$f_x^+$	$f_x^-$	$\Delta f_x$	Atom	$f_x^+$	$f_x^-$	$\Delta f_x$
N0	0.000	-0.02	0.02	C0	-0.017	-0.148	0.131
N1	-0.075	-0.066	-0.009	N1	-0.085	-0.033	-0.052
C2	-0.118	-0.002	-0.116	C2	0.096	-0.063	0.159
N3	-0.06	-0.106	0.046	C3	-0.124	-0.094	-0.03
N4	0.067	-0.065	0.132	C4	0.005	-0.05	0.055
C5	-0.028	-0.016	-0.012	C5	-0.082	0.005	-0.087
C6	0.006	-0.049	0.055	N6	0.037	-0.245	0.282
C7	-0.013	-0.01	-0.003	C7	0.119	0.116	0.003
C8	-0.024	-0.052	0.028	C8	-0.436	-0.157	-0.279
C9	-0.014	-0.036	0.022				
C10	0.018	-0.012	0.030				
C11	-0.006	0.031	-0.037				
C12	-0.024	-0.035	0.011				
C13	-0.048	-0.009	-0.039				
C14	-0.05	-0.021	-0.029				
C15	-0.045	-0.011	-0.034				
C16	-0.03	-0.009	-0.021				
N17	0.034	-0.03	0.064				
C18	0.002	-0.023	0.025				
C19	0.009	0.002	0.007				
C20	-0.029	-0.017	-0.012				
O21	-0.069	-0.043	-0.026				
N22	-0.001	-0.01	0.009				
N23	0.012	-0.007	0.019				
C24	0.017	-0.013	0.030				
C25	0.01	-0.022	0.032				

**Table 11.** ACP and FD MAC calculated FF parameters for the gas-phase.

FD				ACP			
Atom	$f_x^+$	$f_x^-$	$\Delta f_x$	Atom	$f_x^+$	$f_x^-$	$\Delta f_x$
N0	-0.003	-0.011	0.008	C0	-0.02	-0.068	0.048
N1	-0.076	-0.054	-0.022	N1	-0.052	-0.054	0.002
C2	-0.069	-0.017	-0.052	C2	-0.007	-0.048	0.041
N3	-0.020	-0.038	0.018	C3	-0.039	-0.019	-0.02
N4	0.018	-0.066	0.084	C4	-0.013	-0.039	0.026
C5	-0.004	0.007	-0.011	C5	-0.033	-0.006	-0.027
C6	0.004	-0.026	0.030	N6	0.000	-0.121	0.121
C7	-0.001	-0.015	0.014	C7	0.022	0.015	0.007
C8	-0.013	-0.031	0.018	C8	-0.360	-0.174	-0.186
C9	0.001	-0.015	0.016				
C10	0.000	-0.027	0.027				
C11	-0.006	0.002	-0.008				
C12	-0.025	-0.013	-0.012				
C13	-0.003	-0.012	0.009				
C14	-0.044	-0.013	-0.031				
C15	-0.005	-0.012	0.007				
C16	-0.020	-0.008	-0.012				
N17	0.004	-0.009	0.013				
C18	0.035	-0.008	0.043				
C19	0.035	-0.009	0.044				
C20	-0.013	-0.021	0.008				
O21	-0.066	-0.039	-0.027				
N22	-0.01	-0.017	0.007				
N23	-0.003	-0.004	0.001				
C24	0.027	-0.004	0.031				
C25	0.028	-0.005	0.033				

**Table 12.** ACP and FD NBOC FF parameters for the gas phase.

FD				ACP			
Atom	$f_x^+$	$f_x^-$	$\Delta f_x$	Atom	$f_x^+$	$f_x^-$	$\Delta f_x$
N0	-0.011	-0.026	0.015	C0	-0.02	-0.105	0.085
N1	-0.091	-0.07	-0.021	N1	-0.054	-0.03	-0.024
C2	-0.118	-0.009	-0.109	C2	-0.078	-0.089	0.011
N3	-0.021	-0.066	0.045	C3	-0.046	-0.046	0.000
N4	0.007	-0.112	0.119	C4	-0.017	-0.040	0.023
C5	0.009	0.010	-0.001	C5	-0.046	-0.028	-0.018
C6	0.000	-0.043	0.043	N6	-0.017	-0.194	0.177
C7	-0.004	-0.009	0.005	C7	0.022	0.021	0.001
C8	-0.034	-0.07	0.036	C8	-0.352	-0.146	-0.206
C9	0.001	-0.012	0.013				
C10	-0.003	-0.042	0.039				
C11	-0.004	0.015	-0.019				
C12	-0.049	-0.019	-0.03				
C13	-0.002	-0.012	0.01				
C14	-0.100	-0.025	-0.075				
C15	-0.007	-0.011	0.004				
C16	-0.042	-0.011	-0.031				
N17	0.011	-0.043	0.054				
C18	0.026	-0.007	0.033				
C19	0.026	-0.007	0.033				
C20	-0.006	-0.009	0.003				
O21	-0.068	-0.040	-0.028				
N22	-0.012	-0.019	0.007				
N23	0.003	-0.031	0.034				
C24	0.022	-0.005	0.027				
C25	0.021	-0.005	0.026				

**Table 13.** ACP and FD EPC calculated FF parameters for the aqueous phase.

FD				ACP			
Atom	$f_x^+$	$f_x^-$	$\Delta f_x$	Atom	$f_x^+$	$f_x^-$	$\Delta f_x$
N0	0.007	0.009	-0.002	C0	-0.051	-0.154	0.103
N1	-0.102	-0.083	-0.019	N1	-0.104	-0.032	-0.072
C2	-0.152	0.009	-0.161	C2	0.082	-0.069	0.151
N3	-0.075	-0.125	0.05	C3	-0.137	-0.030	-0.107
N4	0.065	-0.154	0.219	C4	-0.034	-0.125	0.091
C5	-0.062	-0.029	-0.033	C5	-0.045	0.050	-0.095
C6	0.013	-0.082	0.095	N6	-0.03	-0.402	0.372
C7	-0.02	-0.015	-0.005	C7	0.092	0.043	0.049
C8	0.018	-0.061	0.079	C8	-0.487	-0.077	-0.410
C9	-0.025	-0.054	0.029				
C10	0.028	-0.032	0.060				
C11	-0.024	0.012	-0.036				
C12	-0.040	-0.014	-0.026				
C13	-0.068	-0.010	-0.058				
C14	-0.017	-0.001	-0.016				
C15	-0.063	-0.01	-0.053				
C16	-0.044	0.004	-0.048				
N17	0.021	0.003	0.018				
C18	-0.032	-0.032	0.000				
C19	-0.023	0.016	-0.039				
C20	-0.047	-0.023	-0.024				
O21	-0.042	-0.025	-0.017				
N22	-0.004	-0.001	-0.003				
N23	-0.002	0.030	-0.032				
C24	-0.003	-0.021	0.018				
C25	-0.012	-0.03	0.018				

**Table 14.** ACP and FD MAC calculated FF parameters for the aqueous phase.

FD				ACP			
Atom	$f_x^+$	$f_x^-$	$\Delta f_x$	Atom	$f_x^+$	$f_x^-$	$\Delta f_x$
N0	0.007	-0.003	0.010	C0	-0.050	-0.083	0.033
N1	-0.128	-0.071	-0.057	N1	-0.072	-0.034	-0.038
C2	-0.108	-0.047	-0.061	C2	-0.078	-0.058	-0.02
N3	-0.053	-0.048	-0.005	C3	-0.099	-0.015	-0.084
N4	0.018	-0.146	0.164	C4	-0.036	-0.088	0.052
C5	-0.057	-0.033	-0.024	C5	-0.022	-0.054	0.032
C6	-0.01	-0.062	0.052	N6	-0.013	-0.216	0.203
C7	0.014	-0.006	0.02	C7	0.015	0.016	-0.001
C8	0.016	-0.012	0.028	C8	-0.387	-0.062	-0.325
C9	0.016	-0.009	0.025				
C10	-0.014	-0.070	0.056				
C11	-0.044	-0.026	-0.018				
C12	-0.067	0.005	0.000				
C13	-0.01	0.013	-0.023				
C14	-0.015	0.022	-0.037				
C15	-0.015	0.015	-0.030				
C16	-0.055	-0.018	-0.037				
N17	-0.01	-0.004	-0.006				
C18	0.005	0.002	0.003				
C19	0.005	0.002	0.003				
C20	-0.008	0.002	-0.01				
O21	-0.050	-0.029	-0.021				
N22	-0.013	-0.003	-0.010				
N23	-0.003	-0.011	0.008				
C24	0.001	0.006	-0.005				
C25	0.001	-0.255	0.256				

**Table 15.** ACP and FD NBOC calculated FF parameters for the aqueous phase.

FD				ACP			
Atom	$f_x^+$	$f_x^-$	$\Delta f_x$	Atom	$f_x^+$	$f_x^-$	$\Delta f_x$
N0	-0.012	-0.012	0.000	C0	-0.037	-0.113	0.076
N1	-0.122	-0.074	-0.048	N1	-0.066	-0.024	-0.042
C2	-0.150	0.000	-0.150	C2	-0.131	-0.091	-0.040
N3	-0.034	-0.085	0.051	C3	-0.072	-0.014	-0.058
N4	-0.006	-0.21	0.204	C4	-0.031	-0.099	0.068
C5	-0.008	0.007	-0.015	C5	-0.048	-0.001	-0.047
C6	-0.005	-0.074	0.069	N6	-0.024	-0.324	0.300
C7	-0.003	-0.005	0.002	C7	0.009	0.008	0.001
C8	-0.009	-0.093	0.084	C8	-0.383	-0.059	-0.324
C9	-0.001	-0.008	0.007				
C10	-0.007	-0.076	0.069				
C11	-0.018	0.003	-0.021				
C12	-0.071	-0.007	-0.064				
C13	-0.011	-0.004	-0.007				
C14	-0.089	-0.009	-0.080				
C15	-0.016	-0.004	-0.012				
C16	-0.063	-0.002	-0.061				
N17	0.003	0.001	0.002				
C18	0.002	0.001	0.001				
C19	0.002	0.001	0.001				
C20	-0.023	-0.004	-0.019				
O21	-0.039	-0.022	-0.017				
N22	-0.015	-0.008	-0.007				
N23	0	0.006	-0.006				
C24	0	0.003	-0.003				
C25	0	0.003	-0.003				

Since FD and ACP behavior was significantly influenced by protonation in the aqueous, gas and aqueous phases, FF were evaluated and applied for the interpretation of the respective reaction sites. The sites of nucleophilic and electrophilic attacks in FD and ACP, for both gas and aqueous phases, were predicted using different FF predictors, including  $f_x^-$ ,  $f_x^+$  and  $\Delta f_x$ . The nucleophilic attacks were at the N(4) and C(7) atoms, in FD and ACP molecules, respectively. The electrophilic attacks were located at the C(20)-O(21) and N(6)-N(7) bonds (which are also the most favorable sites for protonation), for FD and ACP, respectively (Table 16).

**Table 16.** ACP and FD sites for electrophilic and nucleophilic attacks in the gas and aqueous phases.

FF	Gas phase		Aqueous phase	
	FD	ACP	FD	ACP
Nucleophilic (EPC)	N4 ( $f_x^+$ , $\Delta f_x$ )	C7( $f_x^-$ )	N4 ( $f_x^+$ )	C7( $f_x^-$ )
Nucleophilic (MAC)	N4 ( $f_x^+$ , $\Delta f_x$ )	C7( $f_x^-$ , $\Delta f_x$ )	N4 ( $f_x^+$ , $\Delta f_x$ )	C7( $f_x^-$ )
Nucleophilic (NBOC)	N4 ( $\Delta f_x$ )	C7( $f_x^-$ )	N4 ( $\Delta f_x$ )	C7( $f_x^-$ )
Electrophilic (EPC)	O21 ( $\Delta f_x$ )	N6-N7 ( $\Delta f_x$ )	O21 ( $\Delta f_x$ )	N6-N7 ( $\Delta f_x$ )
Electrophilic (MAC)	O21 ( $\Delta f_x$ )	N6-N7 ( $f_x^-$ , $\Delta f_x$ )	O21 ( $\Delta f_x$ )	N6-N7 ( $f_x^-$ )
Electrophilic (NOBC)	O21 ( $\Delta f_x$ )	N6-N7 ( $\Delta f_x$ )	O21 ( $\Delta f_x$ )	N6-N7 ( $\Delta f_x$ )

### Binding energy

The interaction between the inhibitors and the MS surface was evaluated by calculating the binding energy that existed between the formers and the latter, after

merging their optimized structures of the metal crystal (Fig. 9). Equation 25 was adopted to calculate the binding energy between MS and the inhibitors [38]:

$$E_{Bind} (inhibitor-Fe) = E_{Bind(T)} - (E_{Bind(MS)} + E_{Bind(Inhibitor)}) \quad (26)$$

where  $E_{Bind(T)}$  and  $E_{Bind(Inhibitor)}$  are MS and inhibitors total binding energies, respectively. The calculated inhibitors binding energies are shown in Table 17. The results reveal that FD binding energy (12195.39 eV) was lower than that of ACP (63914.25 eV). Therefore, FD average IE (%) was better than that of ACP, because the interaction between the MS surface and FD was stronger than that between the former and ACP.

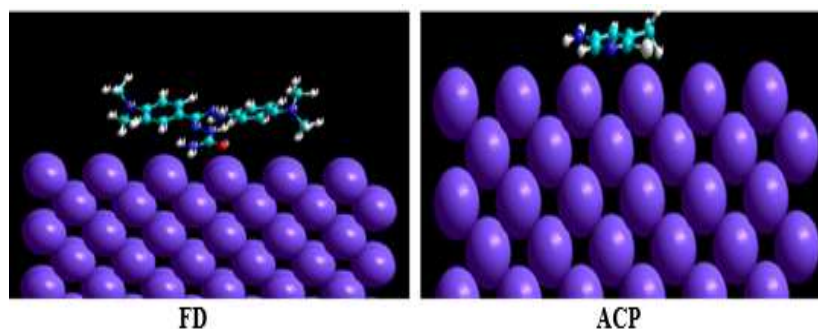


Figure 9. Optimized structures showing MS and inhibitors interaction.

Table 17. Binding and interaction energies between the MS surface and inhibitors.

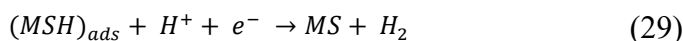
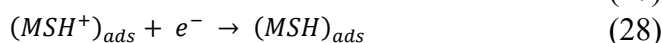
Inhibitor s	$E_{int}(\text{Total})$ (eV)	$E_{bind}(\text{inhib})$ (eV)	$E_{bind}(\text{MS})$ (eV)	$E_{bind}(\text{inhib-MS})$ (eV)
FD	72502.65	-668.61	9257.01	63914.25
ACP	21245.51	-206.89	9257.01	12195.39

### Adsorption mechanism

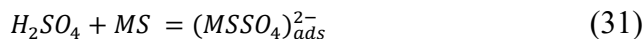
ACP and FD went through chemical adsorption, which involves electrons transfer. One general concept on the adsorption of a corrosion inhibitor is believed to be a displacement of an adsorbed water molecule from the metal surface by the inhibitor, as expressed in Equation 17. However, where other components (such as acidic anions) tend to be adsorbed, this model may not suffice to predict the adsorption mechanism. Therefore, to propose a suitable model, the mechanisms of MS anodic dissolution and the corresponding cathodic HER should be considered. The mechanism for MS anodic dissolution can be presented as follows:



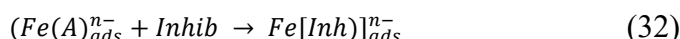
On the other hand, the mechanism for cathodic HER can be written as:



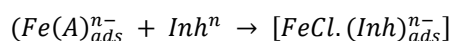
From the above, it is most probably that the initial mechanism was the adsorption of  $\text{HCl}^-$  or  $\text{SO}_4^{2-}$  ions released by the respective acid ionization [39], as shown in the following equations:



However, without inhibitors, the passivation zone will be overcome, and MS will corrode. However, with an inhibitor, further adsorption may involve the anions ( $\text{HCl}^-$  or  $\text{SO}_4^{2-}$ ) displacement (Equation 27a) or joint adsorption onto MS passivating layer (Equation 36):



(33)



where A is the conjugate base of the acid and Inh represents the charged/protonated inhibitor. In the above-proposed mechanism, whichever reaction is favored depends on several factors, especially temperature, protonation degree, etc.

## Conclusions

The results of the present study and the findings drawn therein led to the following conclusions:

1. ACP and FD are good inhibitors for MS corrosion in both HCl and  $\text{H}_2\text{SO}_4$  solutions. Although their IE (%) are relatively comparable, FD seems to perform slightly better than ACP.
2. ACP and FD IE (%) had a strong correlation with calculated quantum parameters, such as FMO energies,  $\sigma$ ,  $\eta$  and  $\Delta N$ .
3. The inhibitors adsorption favored Langmuir's, Temkin's, Freundlich's and Frumkin's isotherms, and presented an energy barrier that suggested mixed type adsorption, with an initial physisorption mechanism.
4. Polarization data confirmed that the inhibitors majorly acted as cathodic, by retarding cathodic HER more than suppressing MS dissolution.  $C_{dl}$  varied inversely with  $R_{ct}$ , and gave a strong signal that the inhibitors were effective against MS corrosion in the acidic media.
5. The protonated inhibitors adsorption seems to have prevailed over the neutral molecules adsorption. FF indices were useful in predicting the inhibitors adsorption sites, and the strong influence of the aqueous environment over the inhibitors reactivity was upheld through calculated aqueous phase data.

## Acknowledgement

The authors acknowledge tertiary education trust fund of Nigeria for providing the computational chemistry calculations through National Research fund, with Professor Nnabuk Okon Eddy as Principal Investigator.

### Authors' contributions

**Anand Balasubramanian:** conceived and designed the analysis; collected the data; inserted data or analysis tools; wrote the paper. **Vidyadharani Gopalakrishnan:** conceived and designed the analysis; collected the data. **Loganathan Subramanian:** conceived and designed the analysis; collected the data. **Rabiu Ibraheem Muhammed:** conceived and designed the analysis; collected the data; inserted data or analysis tools. **Rajni Garg:** inserted data or analysis tools; edited and formatted the paper. **Nnabuk Okon Eddy:** inserted data or analysis tools; performed the analysis; wrote the paper.

### Abbreviations

**AC:** alternating current  
**ACP:** 6-chloro-5-methylpyridin-3-amine  
**AE:** auxiliary electrode  
**C:** concentration  
**C<sub>dl</sub>:** double-layer capacitance  
**CR:** corrosion rate  
**DFT:** density functional theory  
**E:** electric potential  
**EA:** electron affinity  
**E<sub>corr</sub>:** corrosion potential  
**E<sub>HOMO</sub>:** energy of the highest occupied molecular orbital  
**EIS:** electrochemical impedance spectroscopy  
**E<sub>LUMO</sub>:** energy of the lowest unoccupied molecular orbital  
**EPC:** electrostatic potential charges  
**FD:** ((Z)-2-(4-(dimethylamino)phenyl)(2-phenylhydrazinyl)methylene) hydrazinecarboxamide  
**FF:** Fukui function  
**FMO:** frontier molecular orbital  
**GDP:** gross domestic product  
**H<sub>2</sub>SO<sub>4</sub>:** sulfuric acid  
**H<sub>3</sub>PO<sub>4</sub>:** phosphoric acid  
**HCl:** hydrochloric acid  
**HER:** hydrogen evolution reaction  
**HOMO:** energy of the highest occupied molecular orbital  
**I<sub>corr</sub>:** corrosion current density  
**IE (%):** inhibition efficiency  
**IP:** ionization potential  
**k<sub>ads</sub>:** adsorption equilibrium constant  
**k<sub>ads(FK)</sub>:** adsorption-desorption constant  
**LPR:** linear polarization resistant  
**LRD:** local reactivity descriptors  
**LUMO:** energy of the lowest unoccupied molecular orbital  
**MAC:** Mulliken atomic charges  
**MS:** mild steel  
**NBOC:** natural bond orbital charges  
**OCP:** open circuit potential

**PA:** protonation affinity  
**PDP:** potentiodynamic polarization  
**R:** gas constant  
**R<sup>2</sup>:** correlation coefficient  
**R<sub>ct</sub>:** charge transfer resistance  
**RE:** reference electrode  
**R<sub>p</sub>:** polarization resistance  
**SC:** saturated calomel  
**SDF:** spatial data file  
**SEM:** scanning electron microscopy  
**SR:** scanning rate  
**WE:** working electrode  
**WL:** weight loss

### **Symbols definition**

**β<sub>a</sub>:** anodic Tafel constant  
**β<sub>c</sub>:** cathodic Tafel constant  
**ΔE:** energy gap  
**ΔG<sup>o</sup><sub>ads</sub>:** Gibb's free energy of adsorption  
**ΔN:** fraction of electrons transference  
**Δφ:** inner potential difference  
**η:** global hardness  
**θ:** degree of surface coverage  
**μ:** dipole moment  
**σ:** softness  
**χ:** electronegativity

### **References**

1. Bhonge S, Dalwi P, Kulkarni J et al. Recommendations for rehabilitation and corrosion protection of a 100-year-old steel bridge (Durgadee) across heavily polluted river near Mumbai, India. *Rev Alconpat*. 2020;10(2):259-73.
2. Fayomi OSI, Akande IG, Odigie S. Economic Impact of Corrosion in Oil Sectors and Prevention: An Overview. *J Phys Conf Ser*. 2019;1378(2).
3. Bhaskaran R, Palaniswamy N, Rengaswamy NS et al. Global Cost of Corrosion—A Historical Review. In: *Corrosion: Materials* [Internet]. ASM International. 2018:621-8. <https://doi.org/10.31399/asm.hb.v13b.a0003968>
4. Eddy NO, Odoemelam SA. Sparfloxacin and norfloxacin as corrosion inhibitors for mild steel: Kinetics, thermodynamics and adsorption consideration. *J Mater Sci*. 2008;4(1):1-5.
5. Khadom AA, Yaro AS, Altaie AS et al. Electrochemical, activations and adsorption studies for the corrosion inhibition of low carbon steel in acidic media. *Port Electrochim Acta*. 2009;27(6):699-712.
6. Khaled KF. Studies of the corrosion inhibition of copper in sodium chloride solutions using chemical and electrochemical measurements. *Mater Chem Phys*. 2011;125(3):427-33. <http://dx.doi.org/10.1016/j.matchemphys.2010.10.037>
7. Olasunkanmi LO, Idris AO, Adewole AH et al. Adsorption and Corrosion Inhibition Potentials of Salicylaldehyde-based Schiff Bases of Semicarbazide and p-Toluidine on Mild Steel in Acidic Medium: Experimental and Computational Studies. *Surf Interf*. 2020;21:100782. <https://doi.org/10.1016/j.surfin.2020.100782>

8. Eddy NO, Odoemelam SA, Odiongenyi AO. Joint effect of halides and ethanol extract of *Lasianthera africana* on inhibition of corrosion of mild steel in H<sub>2</sub>SO<sub>4</sub>. J Appl Electrochem. 2009;39(6):849-57.
9. Negm NA, Kandile NG, Badr EA et al. Gravimetric and electrochemical evaluation of environmentally friendly nonionic corrosion inhibitors for carbon steel in 1 M HCl. Corros Sci. 2012;65:94-103. <http://dx.doi.org/10.1016/j.corsci.2012.08.002>
10. Abdel-Gaber AM, Abd-El-Nabey BA, Khamis E et al. A natural extract as scale and corrosion inhibitor for steel surface in brine solution. Desalination. 2011;278(1-3):337-42. <http://dx.doi.org/10.1016/j.desal.2011.05.048>
11. Salasi M, Shahrabi T, Roayaei E et al. The electrochemical behaviour of environment-friendly inhibitors of silicate and phosphonate in corrosion control of carbon steel in soft water media. Mater Chem Phys. 2007;104(1):183-90.
12. Ramachandran G, Balamurugan R. Comparative study on mild steel in acidic medium using 5-amino-2-chloro-3-picoline as inhibitor. Asian J Chem. 2018;30(4):917-9.
13. ASTM Standard G-31. Standard Practice for Laboratory Immersion Corrosion Testing of Metals, Annual Book of ASTM Standards. ASTM Int West Conshohocken, USA. 1999;3.02(Reapproved):101.
14. Yurt A, Ulutas S, Dal H. Electrochemical and theoretical investigation on the corrosion of aluminium in acidic solution containing some Schiff bases. Appl Surf Sci. 2006;253(2):919-25.
15. Shainy KM, Rugmini Ammal P, Unni KN et al. Surface Interaction and Corrosion Inhibition of Mild Steel in Hydrochloric Acid Using Pyoverdine, an Eco-Friendly Bio-molecule. J Bio- Tribo-Corros. 2016;2(3):1-12.
16. Rosaline Vimala J, Leema Rose A, Raja S. *Cassia auriculata* extract as corrosion inhibitor for mild steel in acid medium. Int J ChemTech Res. 2011;3(4):1791-801.
17. Hooshmand Zaferani S, Sharifi M, Zaarei D et al. Application of eco-friendly products as corrosion inhibitors for metals in acid pickling processes - A review. J Environ Chem Eng. 2013;1(4):652-7. <http://dx.doi.org/10.1016/j.jece.2013.09.019>
18. Osarolube E, Owate IO, Oforka NC. Corrosion behaviour of mild and high carbon steels in various acidic media. Sci Res Essays. 2008;3(6):224-8.
19. Singh A, Ebenso EE, Quraishi MA. Corrosion inhibition of carbon steel in HCl solution by some plant extracts. Int J Corros. 2012.
20. Dadgarinezhad FB. The inhibition mild steel corrosion in phosphoric acid solutions by 2-phenyl-1-hydrazine carboxamide. J Chil Chem Soc. 2016;3:229-50.
21. Chafiq M, Chaouiki A, Lgaz H et al. Synthesis and corrosion inhibition evaluation of a new schiff base hydrazone for mild steel corrosion in HCl medium: electrochemical, DFT, and molecular dynamics simulations studies. J Adhes Sci Technol. 2020;34(12):1283-314. <https://doi.org/10.1080/01694243.2019.1707561>
22. Aladesuyi O, Fatile BO, Adedapo EA et al. Corrosion Inhibitive Effect of 2-(1-(2-Oxo-2H-Chromen-3-Yl) Ethylidene) Hydrazine Carboxamide on Zinc-Aluminum Alloy in 1.8 M Hydrochloric Acid. Int J Adv Res Chem Sci. 2016;3(2):15-21.
23. Farahati R, Behzadi H, Mousavi-Khoshdel SM et al. Evaluation of corrosion inhibition of 4-(pyridin-3-yl) thiazol-2-amine for copper in HCl by experimental and theoretical studies. J Mol Struct. 2020;1205:127658. <https://doi.org/10.1016/j.molstruc.2019.127658>

24. Zhang J, Zhang J, Zhu F et al. Improved Synthesis of 6-Chloro-5-methylpyridin-2-amine: A Key Intermediate for Making Lumacaftor. *Org Process Res Dev.* 2020;24(6):1175-9.
25. Abd El Rehim SS, Sayyah SM, El-Deeb MM et al. Adsorption and corrosion inhibitive properties of P(2-aminobenzothiazole) on mild steel in hydrochloric acid media. *Int J Ind Chem.* 2016;7(1):39-52.
26. Deyab MA, Essehli R, El Bali B. Inhibition of copper corrosion in cooling seawater under flowing conditions by novel pyrophosphate. *RSC Adv.* 2015;5(79):64326-34. <http://dx.doi.org/10.1039/C5RA08119J>
27. Lai C, Xie B, Zou L et al. Adsorption and corrosion inhibition of mild steel in hydrochloric acid solution by S-allyl-O,O'-dialkyldithiophosphates. *Results Phys.* 2017;7:3434-43. <http://dx.doi.org/10.1016/j.rinp.2017.09.012>
28. Saeed MT, Saleem M, Usmani S et al. Corrosion inhibition of mild steel in 1 M HCl by sweet melon peel extract. *J King Saud Univ Sci.* 2019;31(4):1344-51. <https://doi.org/10.1016/j.jksus.2019.01.013>
29. Ameh P, Ebenso E, Eddy NO et al. Corrosion Inhibition Potential of *Daniella oliverri* Gum Exudate for Mild Steel in Acidic Medium. 2012;7(July):7425-39. [www.electrochemsci.org](http://www.electrochemsci.org)
30. Ogunleye OO, Arinkoola AO, Eletta OA et al. Green corrosion inhibition and adsorption characteristics of *Luffa cylindrica* leaf extract on mild steel in hydrochloric acid environment. *Heliyon.* 2020;6(1):e03205. <https://doi.org/10.1016/j.heliyon.2020.e03205>
31. Chokkalingam M, Singh P, Huo Y et al. Facile synthesis of Au and Ag nanoparticles using fruit extract of *Lycium chinense* and their anticancer activity. *J Drug Deliv Sci Technol.* 2019 Feb;49:308-15. <https://doi.org/10.1016/j.jddst.2018.11.025>
32. Pilepi V, Urši S. Nucleophilic reactivity of the nitroso group. Fukui function DFT calculations for nitrosobenzene and 2-methyl-2-nitrosopropane. *J Mol Struct.* 2001;538:41-9.
33. Xu X, Singh A, Sun Z et al. Theoretical, thermodynamic and electrochemical analysis of biotin drug as an impending corrosion inhibitor for mild steel in 15% hydrochloric acid. *R Soc Open Sci.* 2017;4(12).
34. Alhaffar MT, Umoren SA, Obot IB et al. Isoxazolidine derivatives as corrosion inhibitors for low carbon steel in HCl solution: Experimental, theoretical and effect of KI studies. *RSC Adv.* 2018;8(4):1764-77.
35. Perea-Ramírez LI, Guevara-García A, Galván M. Using local softness to reveal oxygen participation in redox processes in cathode materials. *J Mol Model.* 2018;24(9):0-8.
36. Gao L, Peng S, Gong Z et al. A combination of experiment and theoretical methods to study the novel and low-cost corrosion inhibitor 1-hydroxy-7-azabenzotriazole for mild steel in 1 M sulfuric acid. *RSC Adv.* 2018;8(67):38506-16.
37. Eddy NO, Ita BI. Experimental and theoretical studies on the inhibition potentials of some derivatives of cyclopenta-1,3-diene for the corrosion of mild steel in HCl solutions. *Int J Quantum Chem.* 2011;111(14):3456-74.
38. Eddy NO, Momoh-Yahaya H, Oguzie EE. Theoretical and experimental studies on the corrosion inhibition potentials of some purines for aluminum in 0.1 M HCl. *J Adv Res.* 2015;6(2):203-17. <http://dx.doi.org/10.1016/j.jare.2014.01.004>
39. Roling LT, Abild-Pedersen F. Structure-Sensitive Scaling Relations: Adsorption Energies from Surface Site Stability. *Chem Cat Chem.* 2018;10(7):1643-50.